Title

Graphene K-Tape Meshes for Densely Distributed Human Motion Monitoring

Journal

Advanced Materials Technologies, 6(1)

ISSN

2365-709X

Authors

Lin, Yun-An
Zhao, Yingjun
Wang, Long
et al.

Publication Date

2021

DOI

10.1002/admt.202000861

Peer reviewed

DOI: 10.1002/ (manuscript number))
Article type: Communication

Graphene K-Tape Meshes for Densely Distributed Human Motion Monitoring

*Yun-An Lin, Yingjun Zhao, Long Wang, Yujin Park, Yi-Jui Yeh, Wei-Hung Chiang, and Kenneth J. Loh**

Y-A. Lin, Dr. Y. Zhao, Dr. L. Wang, and Prof. K. J. Loh
University of California San Diego, Department of Structural Engineering, Active, Responsive, Multifunctional, and Ordered-materials Research (ARMOR) Lab, 9500 Gilman Dr MC 0085, La Jolla, CA 92093-0085, USA
*E-Mail: kenloh@ucsd.edu

Dr. Y. Zhao
DoD-VA Extremity Trauma and Amputation Center of Excellence (EACE), Naval Medical Center San Diego, San Diego, CA 92134, USA

Y. Park and Prof. K. J. Loh
University of California San Diego, Materials Science & Engineering, 9500 Gilman Dr MC 0418, La Jolla, CA 92093-0418, USA

Y-J. Yeh and Prof. W-H. Chiang
National Taiwan University of Science and Technology, Department of Chemical Engineering, No. 43, Sec. 4, Keelung Rd., Taipei 106, Taiwan

Keywords: fabric, electrical impedance tomography, kinesiology tape, muscle, nanocomposite, physiological monitoring, strain sensor, thin film, wearable

Abstract: Wearable sensors that measure parameters associated with physical activity and bodily motions have been regarded as an indispensable tool for assessing personal wellness. Recent advances in nanocomposite strain sensors have been successfully used for monitoring skin strains and other strain-derived physiological parameters. This study complements the existing body of work and presents a flexible, self-adhering, fabric-based wearable sensor for measuring skin strains and human motions. Graphene nanosheet thin films are directly spray-coated onto kinesiology tape (K-Tape) to obtain a self-adhering strain sensor of high sensitivity and linearity. Their stable sensing performance and high repeatability are verified, while human subject tests confirm that they adequately capture muscle engagement during functional movements. In addition, densely distributed strain monitoring can be achieved using an electrical impedance tomography measurement approach and algorithm. Spatial strain sensing

is successfully demonstrated using a single strip of piezoresistive K-Tape, as well as when a K-Tape network or mesh pattern is formed. The results show promise for using graphene K-Tape meshes to measure how specific major muscle groups engage during different physical activities.

Manuscript:

The health benefits of physical activity and exercise are well recognized in medicine,[1] while inactivity and living a sedentary lifestyle can contribute to higher disease risk factors.[2] These risks increase with aging and are worsened by the global obesity epidemic.[3] At the other end of the spectrum, athletes and military service members that undergo intense physical training and recreational activities can suffer severe overuse injuries.[4] Therefore, the ability to accurately monitor the range, amplitude, and quality of bodily movements is critical for promoting behavioral changes that yield higher levels of activity, maintaining and enhancing personal wellness, improving functional performance, preventing debilitating musculoskeletal injuries, and facilitating active rehabilitation.

Wearable sensors that measure parameters associated with physical activity and bodily motions have been regarded as an indispensable tool for assessing personal wellness. Among its ~ 350 million users worldwide (in 2019),[5, 6] mainstream commercialized wearables pack force transducers, gyroscopes,[7] accelerometers,[8] and magnetometers in a hardcase accessory,[9] such as watches or bracelets,[10-12] to record vital signs (*e.g.*, heart rate, respiration rate, peripheral oxygen saturation, and body temperature) and physical activity (*e.g.*, steps). Despite their prevalence, they offer limited accuracy[13-15], and their large, rigid, and bulky form factors can cause user discomfort or inconvenience, especially for the elderly. Recent advances in flexible sensors allow them to be worn at locations where traditional devices would otherwise be unsuitable or challenging because of their limited stretch-ability.[16] One approach is to

integrate soft and flexible elastomeric sensors with fabric to monitor vitals and physiological parameters[17], garments to measure hip, knee, and ankle kinematics,[18] and gloves to monitor finger motion, pressure, and tensile forces.[19] However, movement- and motion-induced strains in skin may not be effectively nor accurately measured by garment-based sensors due to poor strain transfer.

An alternative is to use high-performance, stretchable, elastomeric strain sensors[20] (*e.g.*, using nanomaterials including silver nanoparticles[21] or aligned single-walled carbon nanotubes[22]) mounted directly onto skin. In particular, graphene possesses extraordinary mechanical, thermal, and electrical properties,[31] and many sensors based on graphene exhibit superior sensing performance thanks to their topology-dependent, strain-sensitive, electromechanical properties.[32-34] For instance, a pulse monitor formed by integrating a crisscross graphene woven fabric with polydimethylsiloxane (PDMS) thin film and 3M adhesive tape exhibits ultra-high gage factor, which enables monitoring of critical features in the pulse waveform.[35] Other examples include stretchable graphene oxide (GO) yarns[23] and engraved octopus-inspired microsuckers based on reduced GO fabrics in elastomers.[24] Such skin-mounted ultrathin nanocomposites can reliably capture finger-bending movements,[25] heartbeat and respiration,[26] and eye blinks and radial pulse.[27] Similarly, flexible tattoo-like sensors that integrated smart materials (*e.g.*, polyvinylidene fluoride piezo-polymers or gold-silver nanocomposites) with serpentine-structured interconnects and skin-like medical tape have also been developed.[28-30] Another study has utilized a fish scale-like graphene-based sensing layer and demonstrated high sensitivity, stability, and broad sensing range for applications ranging from detecting vitals to monitoring joint-bending motions.[36]

Despite these advances, most wearable measurands only provide a global sense of physical wellbeing[37] and are unable to monitor specific muscle groups or complex limb motions.[38]

Many sensor designs and fabrication processes are also sophisticated, which may be difficult to scale. More importantly, most state-of-the-art wearables rely on discrete transducers that only measure data where they are instrumented,[39] and full-field physical monitoring still requires many sensors, not to mention the associated cabling and data acquisition requirements.

In this study, we introduce a method for capturing distributed muscle engagement and skin strains using flexible, self-adhering, fabric-based, wearable sensors. The approach is to integrate strain-sensitive graphene nanosheet (GNS) thin films with kinesiology tape (K-Tape) as the substrate. K-Tape, which is a unidirectionally stretchable and self-adhering fabric strip, is already being used for muscular injury prevention and recovery by directly affixing them in unique patterns over major muscle groups.[40] GNS is employed for nanocomposite design, because these strain sensors exhibit higher sensitivities, repeatability, and minimal drift as compared to ones based on other nanomaterials such as carbon nanotubes. In addition to designing a unidirectionally stretchable wearable sensor, the significance of this study is that these “Graphene K-Tapes” can directly measure distributed strains when interrogated using an electrical impedance tomography (EIT) measurement technique and conductivity reconstruction algorithm.

The fabrication process of Graphene K-Tape is illustrated in Figure 1(a). GNS, which is synthesized using water-assisted liquid-phase exfoliation (WALPE),[41] is dispersed in an ethyl cellulose (EC) solution. Then, the GNS-EC ink is airbrushed onto the exposed rectangular region of a masked K-Tape substrate. The scanning electron microscope (SEM) image in Figure 1(b) shows that GNS-EC is deposited over all individual fabric fibers, as opposed to forming a thick continuous film over the fabric. Integration of the film with each fiber enables the nanocomposite to deform with the fabric without delaminating, especially under large and repeated cyclic strains. The high-resolution SEM image in Figure 1(c) confirms that GNS are

effective dispersed, deposited, and characterized by a percolated morphology of overlapping flat nanosheets.

The mechanical properties of bare versus Graphene K-Tape are investigated by straining them to 100% in monotonic uniaxial tension (Figure 1(d) inset). Figure 1(d) plots their stress-strain responses and confirms their nearly identical stress-strain properties, before deviating more significantly after ~ 70% strain. More importantly, the GNS-EC thin films do not alter the instantaneous stiffness of K-Tape by more than 10% throughout the entire loading history nor does it adversely affect its mechanical performance, stretch-ability, and functionality. In practice, when K-Tape is used on the body, the expected strains are well below 70%.[42]

The effects of applied strains on GNS microstructure are characterized by micro-Raman spectroscopy. Figure 1(e) overlays the Raman spectra of a specimen subjected to uniaxial tensile strains from 0% to 10%, and all cases show the three typical GNS peaks (*i.e.*, the D, G, and 2D bands at 1340, 1577, and 2692 cm^{-1}, respectively). The low intensity ratio of the D to G bands (I_D/I_G) of 0.03 and high 2D peak intensity for the unstrained case confirm that as-deposited GNS have few defects. Figure 1(e) also shows that I_D/I_G decreases with increasingly applied tensile strains, indicating strain-induced disruption of the GNS microstructure network. In addition, three-dimensional (3D) micro-Raman of a Graphene K-Tape strained to 1% reveals the Raman spectra of the specimen probed at different Z depths (Figure 1(f)). The clear reduction of G band intensity suggests that GNS-EC films are well-integrated with the fabric fibers, where the film thickness is ~ 5 to 15 μm. In addition, Figure 1(g) compares how I_D/I_G increases with depth when the specimen is strained to 1% and 10%. Both Raman spectra exhibit the same trend, where higher I_D/I_G at greater depths may be due to a lower-density GNS network at the fabric interface, again, suggesting that GNS-EC is absorbed and infused into the fabric. Nevertheless, Figure 1(g) confirms that strains are uniformly applied to the entire GNS-EC thin

film, since a uniform change in I_D/I_G is observed across all depths when greater strains (10%) are applied. Furthermore, micro-Raman spectra of the Graphene K-Tape before and after 200 cycles of loading are plotted in Figure 1(h). The 2D-band intensity and I_D/I_G value remain stable over multiple stretching cycles, indicating no apparent damage due to straining.

After confirming strain-induced morphological changes in the GNS-EC network, the strain sensing properties of Graphene K-Tape are characterized via uniaxial tensile and cyclic tests while simultaneously measuring their electrical resistance response. Figure 1(i) plots an overlay of resistance as a function of strain for four consecutive monotonic tensile tests conducted at 0.02, 0.05, 0.10, and 0.50 mm/s. The similar responses obtained indicate that Graphene K-Tape do not exhibit rate-dependent electromechanical behavior at these strain rates. In addition, their sensing response is linear up to ~ 10% strain. Future improvements are needed if they are to be applied at bodily locations that undergo significant strains.

Their strain sensitivity (S) or gage factor is then characterized by computing and plotting normalized change in resistance (R_n) versus applied strains in Figure 1(i). The slope of the linear least-squares regression line fitted to the data from each load cycle is equivalent to S:

$$S = \frac{{}^{R_i - R_0}/_{R_0}}{\Delta\varepsilon} \quad (1)$$

where R_0 is unstrained resistance at 0%, and R_i is resistance due to applied strain ($\Delta\varepsilon$). Separate linear regression lines are fitted to each test data, and the calculated sensitivities are similar and with an average of ~ 95.9. Figure 1(j) shows a representative resistance time history of a Graphene K-Tape subjected to 200 tension cycles to a peak strain of 3%. Overall, the cyclic electromechanical response exhibits high stability and closely follows the strain pattern with minimal drift, as is evident from Figures 1(j) and 1(k). In addition, complete recovery of initial resistance is observed, where its resistance after each unloading cycle is nearly constant. This

result is in stark contrast with many flexible polymer nanocomposites, which are viscoelastic and exhibits undesirable baseline resistance drift when cyclically loaded. However, Figure 1(j) shows that resistance increase is greater during the first several cycles of loading (~ 10) before eventually stabilizing, which may be due to initial stress relaxation of K-Tape and EC matrix. Nonetheless, separate linear regression lines are fitted to each loading cycle dataset for all 200 cycles (Figure 1(l)). The average S is ~ 70.0, and the average coefficient of determination (R^2) is 0.9944, which confirms strong sensor linearity.

Human subject validation tests are then conducted by affixing Graphene K-Tape onto the wrist. The sensor is initially mounted when the wrist is unbent, with the back of the hand and forearm forming a straight line (Figure 2(a) inset). The entire movement test is also captured by video, and a representative resistance time history is plotted in Figure 2(a), where repeatable and stable response is observed. Video frames from a cycle of wrist-bending motion are extracted (Figure 2(b)) and then analyzed by image processing to compute the instantaneous wrist angles. The angle and resistance time histories are overlaid in Figure 2(c) and show good agreement. Some differences are observed, potentially because wrist bending only strains the midsection of the long strip of Graphene K-Tape, so only a portion of the film responds with significant resistance changes that contributes to overall sensor nonlinearity. Nevertheless, Figures 2(a) and 2(c) show that Graphene K-Tape can be used for sensing both tensile and compressive skin strains.

To further demonstrate its use for monitoring the engagement of different muscle groups, a simple sensing network in the shape of a ‘Y’ is assembled by sewing together three separate pieces of Graphene K-Tape. The Graphene K-Tape network is then mounted to cover a subject’s middle deltoid, posterior deltoid, and triceps. Two-point probe electrical resistance of the three Graphene K-Tape elements in the ‘Y’ are simultaneously measured when the subject performs various controlled exercise routines. Figures 2(d) and 2(e) plot the resistance time

histories when the subject performed repeated push-ups and triceps dips, respectively. Each resistance time history shows high repeatability and stability with minimal drift. For each physical activity, the disparate waveforms corresponding to different Graphene K-Tape elements in the network reflect the engagement of specific muscle groups at different instances throughout the functional motion sequence. In general, each sensor strip experiences an increase or decrease in resistance when the muscle group underneath is extending or contracting, respectively.

In typical sports medicine and rehabilitation practices, multiple strips of K-Tape are applied to form an interconnected mesh- or grid-like pattern.[43-46] The results presented insofar successfully validate that fabrics can be engineered to measure muscle and skin strains. However, as the complexity of Graphene K-Tape networks or "meshes" grows, the simultaneous data acquisition of all sensing elements becomes more complicated and burdensome. Furthermore, only the average strain (or resistance) of each Graphene K-Tape element is resolved by two-point probing. Yet, every location of the GNS-EC thin film is sensitive to strain. To fully utilize the entire nanocomposite as a densely distributed strain sensor, we introduce an EIT measurement technique and algorithm[47] that can reconstruct the conductivity (or resistivity) distribution of the entire Graphene K-Tape using only a limited number of measurements acquired at the boundary. Like many tomographic methods, EIT provides much higher spatial imaging and sensing resolution while using much fewer electrodes (and cabling) than direct two-point probing of the same area.

EIT is a soft-field imaging technique used in numerous biomedical and structural health monitoring applications, primarily for visualizing, detecting, and localizing anomalies.[48-51] The conductivity (*i.e.*, inverse of resistivity) distribution (σ) of a defined body (Ω) can be reconstructed by voltage responses observed along its boundary ($\partial\Omega$).[52-54] When a predefined

electrical field is applied over Ω, the boundary voltage response is unique, assuming that there is no internal current source within Ω. A localized change in conductivity can therefore change the boundary voltage response, since the summation of current density within Ω is zero, or,[47]

$$\nabla \cdot (\sigma \nabla u) = 0 \tag{2}$$

where ∇u is the electrical field within Ω. Equation (2) constitutes the forward calculation when σ is known and when boundary voltage V is sought:

$$V = \nabla u \cdot \boldsymbol{n} \tag{3}$$

where $\boldsymbol{n}$ is the unit vector normal to $\partial\Omega$. However, EIT seeks to determine σ for the entire conductive body using boundary voltages, which requires solving Equation (2) as an inverse problem. Numerical methods such as a finite element (FE) model is usually implemented for solving the weak formulation of Equation (2). The boundary voltage V can be experimentally acquired by measuring voltage potential responses between equidistantly-spaced electrodes instrumented along $\partial\Omega$, and the electrical field over Ω can be induced by injecting a direct current (DC) to one electrode and grounding at another. While current is injected, voltage potentials between all adjacent pairs of electrodes are measured. Multiple sets of unique voltage measurements can be obtained by injecting current between different electrode pairs. The complete electrode model considers the influence from each electrode's contact impedance:

$$\int_{E_l}^{0} \sigma \frac{\partial u}{\partial \boldsymbol{n}} ds = I_l \tag{4a}$$

$$u + z_l \sigma \frac{\partial u}{\partial \boldsymbol{n}} = V_l \tag{4b}$$

where E_l denotes the l^{th} electrode, I_l and V_l are the current and voltage potential over the same electrode, respectively, while z_l represents the electrode's contact impedance. The discrete forms of Equations (2) and (4) constitute the FE problem to be solved. Conventionally, σ is evaluated via iterative least-squares estimation, which can be computationally expensive and extremely sensitive to noise. In this work, a one-step linear inverse solver that calculates the change in conductivity distribution ($\Delta\sigma$) before- and after straining the K-Tape is adopted. In

particular, the maximum *a posteriori* (MAP) method assumes that the empirical condition before and after loading remains identical:[55, 56]

$$\Delta\sigma = (H^T W H + \lambda R)^{-1} H^T W \Delta V \quad (5)$$

where ΔV is the change in boundary voltage response, H is the sensitivity matrix linearly mapping $\Delta\sigma$ to ΔV, and W is the weighing matrix. To smooth out the linear transformation, a Tikhonov regularization matrix R is employed and controlled by the hyperparameter λ. Once the change in conductivity distribution is determined, a calibration curve can be used to convert $\Delta\sigma$ to the physical parameter of interest, such as the change in strain between two states.

Therefore, to demonstrate densely distributed strain sensing, a Graphene K-Tape with 14 boundary electrodes (formed using sewn conductive threads and colloidal silver paste) is adhered onto the subject's knee (Figure 3(a)). A baseline boundary voltage dataset is acquired when the knee is unbent (180°). Then, subsequent EIT boundary voltage datasets are obtained when the knee was bent to different angles, where bending angle is estimated using an XSENS DOT inertial measurement unit. Each of these datasets, as well as the unbent baseline case, are used as inputs for the EIT inverse problem to reconstruct the conductivity distribution of the Graphene K-Tape. Figure 3(b) shows a representative set of EIT results, where each EIT image is the change in conductivity distribution of the specimen with respect to when the knee was unbent. Figure 3(b) shows that the middle portion of the Graphene K-Tape (*i.e.*, corresponding to the region above the kneecap) decreases in conductivity as bending angle increases, straining the skin in tension.

A similar EIT test is performed with a smaller Graphene K-Tape (with eight boundary electrodes) mounted onto a subject's wrist. By bending the wrist back and forth, similar to Figure 2(b), both localized tension and compression are induced at the wrist joint. The corresponding conductivity maps shown in Figure 3(c) verify that EIT can capture the

magnitudes and locations where localized compressive and tensile strains are induced during wrist bending.

In addition to identifying the locations and magnitudes of skin strains, muscle engagement monitoring during different functional movements also requires sensing the directionality of strains when Graphene K-Tapes are mounted over major muscle groups. Therefore, we have designed “Graphene K-Tape Meshes” in the shape of an elongated hexagon, which resemble a truss-like structure with interconnected high aspect ratio Graphene K-Tape elements or struts as shown in Figure 3(d). The shape of this mesh is inspired by how K-Tape strips are applied over major limbs and joints, such as the leg and knee. In practice, the geometry and design of Graphene K-Tape Meshes can be tailored to the specific region of interest. Each strut in the hexagonal pattern is labeled according to Figure 3(e), where ‘D’ is for diagonal and ‘H’ is for horizontal elements. Graphene K-Tape Meshes are fabricated by pre-cutting a large, bare, K-Tape to form the desired pattern, before spray-coating the GNS-EC nanocomposite. Six conductive thread electrodes are sewn at the interconnecting nodes along the specimen’s boundaries (Figure 3(d)). Then, distributed strain sensing is validated by affixing the Graphene K-Tape Mesh onto a polyethylene terephthalate (PET) substrate and conducting monotonic, uniaxial, tensile testing in the vertical direction (Figure 3(d)). EIT boundary voltage measurements are obtained at every 0.5% interval and up to a peak strain of 2.0% to prevent plastic deformation of PET. Voltage measurements for each strain state, as well as for the baseline unstrained case, are used as inputs for solving the EIT inverse problem.

Figure 3(f) shows a representative set of EIT results that map the Graphene K-Tape Mesh’s change in conductivity with respect to its unstrained state. As expected, Figure 3(f) shows that all the diagonal D1 to D8 struts decrease in conductivity in response to tensile strains. Similarly, horizontal H1 to H4 elements increase in conductivity due to compression because of Poisson’s

effect. These results are consistent with the electromechanical properties of Graphene K-Tape shown in Figure 1(k). However, the bottom half of the Graphene K-Tape Mesh seems to respond more significantly to strains, while the top half started with a large change in conductivity even at low levels of applied strains. This may be due to slight misalignment and pre-tensioning of the top half of the Graphene K-Tape Mesh during initial specimen mounting. Nevertheless, closer examination of these EIT results in Figure 3(f) show that the diagonal elements experience a decrease in conductivity (or increase in resistivity) in tandem with increasing tensile strains. The exception to this is the D4 strut; when strained to 1.5%, the change in conductivity is close to 0. This may have been due to poor adhesion of the D4 strut to the PET substrate, which then delaminated when strained to 1.5%. For the horizontal elements, H2 to H4 show an expected and consistent increase in conductivity (or decrease in resistivity) with increasing applied tension.

Upon validating distributed strain sensing through load testing, a Graphene K-Tape Mesh was also affixed over a subject's biceps, and EIT datasets are obtained when the subject's biceps are relaxed and flexed (Figure 3(g). The change in conductivity map in Figure 3(h) show that the conductivities of H1 to H4 all decrease due to tension caused by flexing of the biceps. The opposite response is observed along the direction of the arm, where flexing induces compression and thus an increase in conductivity (or decrease in resistivity) of D1 to D8. Overall, the pattern of the EIT conductivity map matches physical observations during testing and agrees with previous results shown in Figures 1(k) and 2(c). Furthermore, one can also observe significant conductivity changes near H4 and the right-hand-side portions of D2, D4, D7, and D8 (*i.e.*, near *(ii)* in Figure (3(f)). When the biceps are flexed, the subject's skin near the elbow wrinkles due to significant local compression, and this response is captured by the EIT result in Figure 3(h). Compressive strain concentrations at the interconnecting strut nodes at the top and bottom of the Graphene K-Tape Mesh are also revealed in Figure 3(h).

In summary, we present in this work self-adhering Graphene K-Tape that functions as a low-profile, highly stretchable, wearable strain sensor. Tensile cyclic load tests have confirmed their stable, repeatable sensing behavior, and their strain sensitivity or gage factor ranges from ~ 70 to 95 depending on film fabrication parameters. When applied over major muscle groups in subjects' limbs, the results confirm that muscular engagement during different functional movements can be accurately monitored. Moreover, densely distributed strain and strain field monitoring are successfully demonstrated by coupling continuous and patterned Graphene K-Tape with an EIT measurement technique and inverse algorithm. Due to the unidirectional stretch-ability of K-Tape, custom-made networks can be designed and affixed onto the body according to one's anatomical structure. Graphene K-Tape Meshes enable unidirectional strain magnitude mapping along each of its struts without being significantly affected by Poisson's effect. Overall, these Graphene K-Tape sensors complement the rich body of work on wearable sensors, while EIT offers a unique and efficient method for extracting distributed human motion information from piezoresistive nanocomposites. To the best of our knowledge, this is the first time where patterned nanocomposite sensors and EIT are used together for densely distributed skin-strain monitoring. Based on these findings, we believe that the visualization of strain distribution during functional movements can be insightful for physical therapy, rehabilitation, personal training, sports medicine, and mobility disability applications.

Additional work is needed before Graphene K-Tape can be deployed for personal use or in healthcare settings. Future work will focus on charactering the accuracy of distributed skin-strain monitoring and comparing the results with an industry gold standard such as digital image correlation. Understanding how Graphene K-Tapes respond to tri-planar joint rotations and how they correlate with motion capture measurements will enable even broader healthcare, fitness, and visual arts applications.

Experimental Methods

GNS-EC Solution: As-synthesized GNS were used for preparing the sprayable ink. Ethyl cellulose was added to 200 proof ethanol to obtain a 2 *wt*.% EC-ethanol solution, followed by 24 h of continuous stirring. GNS was then added to the EC-ethanol solution at a concentration of 15 mg/mL, and the solution was bath sonicated for 2 h (150 W, 22 kHz). Next, the viscosity of the dispersion was adjusted by heating to 60 °C for ~ 12 min using a digital hotplate to allow a portion of ethanol to evaporate. The sprayable GNS-EC ink was obtained once the solution cooled to room temperature.

Graphene K-Tape Fabrication: Prior to spray-coating the nanocomposite, the non-adhesive side of K-Tape was masked to define and form a specific rectangular region for film deposition. A Paasche airbrush was then employed to manually spray-coat the GNS-EC ink onto the exposed region of the K-Tape. A total of three film layers were deposited, pausing ~ 2 min in between each layer to allow the ink to dry completely. The final step then entailed drop-casting, using a pipette, a thin trace of GNS-EC ink over the spray-coated film and allowing the entire specimen to dry for at least 1 h. Drop-casting was performed to allow the GNS-EC ink to enhance the overall uniformity and electrical conductivity of the nanocomposite. The final step involved forming electrodes at appropriate locations on the specimen (*e.g.*, at opposite ends to form a two-point probe measurement setup). Conductive threads were sewn into and over the nanocomposite and K-Tape. A thin dab of colloidal silver paste (Ted Pella) was applied on top of the sewn threads and film for minimizing contact impedance.

Imaging and Spectroscopy: High resolution field-emission SEM (HR-SEM) was conducted with a JEOL JSM-7900F scanning electron microscope. Micro-Raman scattering studies were carried out at ambient condition with a confocal micro-Raman spectrometer (JASCO NRS 5100)

equipped with a 532 nm laser excitation. The spectrometer was carefully calibrated by the silicon band at 520 cm^{-1} using a silicon wafer. Its laser power was maintained at 0.45 mW for a 5-s acquisition time throughout the experiment to avoid thermal effects. Spectra were background subtracted and averaged from 100 random positions on each specimen. In addition, 3D micro-Raman measurement was conducted by repeating the measurements at different *Z*-positions.

Mechanical Characterization: Monotonic, displacement-controlled, uniaxial tensile tests were performed on bare rectangular (~ 25×100 mm^2) K-Tape and Graphene K-Tape specimens using a Test Resources 100R load frame. Each specimen was strained to 100% at a constant loading rate of 0.1 mm/s. The load frame's crosshead displacements and applied load were recorded at 10 Hz. Specimen dimensions were measured using a digital caliper.

Sensing Characterization: Graphene K-Tape specimens were subjected to monotonic, uniaxial, tensile tests (to peak strains of 1% to 15% at a constant loading rate of 0.1 mm/s) and tensile cyclic tests (200 cycles to a peak strain of 3%) using a Test Resources 100R load frame while simultaneously measuring their two-point probe electrical resistance. Besides recording the load frame's crosshead displacement and applied load during these electromechanical tests at 10 Hz, electrical resistance of each specimen was recorded using a Keysight 34465A digital multimeter (DMM) sampling at ~ 1.5 Hz.

Human Subject Testing: The human subject study was approved by the University of California San Diego, Institutional Review Boards, Human Research Protection Program, under Project #191806X, and informed written consent was obtained from all subjects. First, Graphene K-Tape was affixed onto the wrists of human subjects for bending motion monitoring. The wearable sensor was initially mounted when the wrist was unbent (0^o), with the back of the

hand and forearm forming a straight line. Then, the subject slowly bent the wrist downwards until a maximum range of motion was reached, before returning past the initial position and bending upwards until a maximum range of motion was reached again. The entire motion was performed at approximately the same rate. This wrist bending motion was repeated several times, while the Keysight 34465A DMM sampled electrical resistance at ~ 1.5 Hz. The entire movement test was captured using video, and individual frames were extracted during image processing to quantify the angle of rotation of the wrist. Second, three separate pieces of Graphene K-Tape were sewn together using conductive threads to form a network the shape of a 'Y', which was then affixed onto the subjects' middle deltoid, posterior deltoid, and triceps area. The subject performed various controlled physical activities, including push-up, triceps dips, lateral shoulder raises, and punching motions. Two-point probe resistance of the three Graphene K-Tape elements in the 'Y' were simultaneously interrogated using a Keysight 34980A multifunctional switch with a built-in DMM sampling at ~ 8 Hz.

Densely Distributed Strain Monitoring using EIT: Four sets of tests were conducted to validate densely distributed strain monitoring using Graphene K-Tape Meshes. The first test entailed adhering a Graphene K-Tape over a subject's knee. Controlled knee bending was performed while EIT measurements were obtained. The second test was similar, except that the Graphene K-Tape was affixed on the wrist, and both tension and compression were induced while the wrist was bent back and forth. The third test was done by attaching the Graphene K-Tape Mesh onto a polyethylene terephthalate (PET) sheet. Uniaxial, monotonic, tensile tests were performed using a Test Resources 100R load frame. Specimens were stretched at a constant loading rate of 0.1 mm/s to a peak strain of 2.0%, pausing at 0.5% intervals to allow time for EIT measurements. The fourth test affixed a Graphene K-Tape Mesh onto a subject's biceps, followed by performing repeated bicep curls. During both tests, a customized DAQ system

consisting of a Keithley 6221 current generator and a Keysight 34980A multifunctional switch was employed for applying EIT excitations and acquiring boundary voltage measurements.

Acknowledgements

This work was supported by the U.S. Office of Naval Research (ONR) under grant no. N00014-20-1-2329. Partial support was provided to K.J.L. by the 2020 ONR Summer Faculty Research Program (SFRP) made possible by grant no. N00014-18-1-2728. K.J.L. gratefully acknowledges the collaboration of LCDR Dr. John Fraser, Dr. Pinata Sessoms, and Dr. Amy Silder from the Naval Health Research Center (NHRC) in San Diego, California, USA. Y.Z. was supported in part by an appointment to the Department of Defense (DOD) Research Participation Program administered by the Oak Ridge Institute for Science and Education (ORISE) through an interagency agreement between the U.S. Department of Energy (DOE) and the DOD. ORISE is managed by ORAU under DOE contract number DE-SC0014664. All opinions expressed in this paper are the authors' and do not necessarily reflect the policies and views of DOD, DOE, or ORAU/ORISE.

Conflicts of Interest

The authors declare no conflicts of interest.

References

[1] D. E. R. Warburton, S. S. D. Bredin, *Curr Opin Cardiol* **2017**, 32, 541.
[2] T. D'Isanto, A. Manna, G. Altavilla, *Sport Science* **2017**, 10, 100.
[3] S. C. Wearing, E. M. Hennig, N. M. Byrne, J. R. Steele, A. P. Hills, *Obesity Reviews* **2006**, 7, 239.
[4] M. Lovalekar, J. P. Abt, T. C. Sell, D. E. Wood, S. M. Lephart, *Military Medicine* **2016**, 181, 64.
[5] G. Aroganam, N. Manivannan, D. Harrison, *Sensors* **2019**, 19, 1983.
[6] Statista, Wearbles Digital Market Outlook, https://www.statista.com/outlook/319/100/wearables/worldwide, April, 2020.

[7] Y. P. Lim, I. T. Brown, J. C. T. Khoo, in *2008 30th Annual International Conference of the IEEE Engineering in Medicine and Biology Society*, IEEE, Vancouver, BC, Canada **2008**.
[8] A. Jalal, M. A. K. Quaid, K. Kim, *Journal of Electrical Engineering & Technology* **2019**, 14, 1733.
[9] A. Pantelopoulos, N. G. Bourbakis, *IEEE Transactions on Systems, Man, and Cybernetics* **2010**, 40, 1.
[10] P. A. Derchak, L. Czapla, C. A. Rogan, US9801583B2 **2017**.
[11] Frank Mokaya, P. Zhang, US10130298B2 **2018**.
[12] S. Q. Liu, J. C. Zhang, R. Zhu, *IEEE Transactions on Biomedical Engineering* **2019**, 67, 940.
[13] F. A. Storm, B. W. Heller, C. Mazzà, *PLoS One* **2015**, 10,
[14] S. O'Connell, G. ÓLaighin, L. R. Quinlan, *PloS one* **2017**, 12, 1.
[15] K. Price, S. R. Bird, N. Lythgo, I. S. Raj, J. Y. L. Wong, C. Lynch, *Journal of Medical Engineering & Technology* **2017**, 41,
[16] A. Nag, S. C. Mukhopadhyay, J. Kosel, *IEEE Sensors Journal* **2017**, 17, 3949.
[17] C. Gopalsamy, S. Park, R. Rajamanickam, S. Jayaraman, *Virtual Reality* **1999**, 4, 152.
[18] Y. Mengüç, Y.-L. Park, H. Pei, D. Vogt, P. M. Aubin, E. Winchell, L. Fluke, L. Stirling, R. J. Wood, C. J. Walsh, *The International Journal of Robotics Research* **2014**, 33, 1748.
[19] A. Atalay, V. Sanchez, O. Atalay, D. M. Vogt, F. Haufe, R. J. Wood, C. J. Walsh, *Advanced Materials Technologies* **2017**, 2, 1.
[20] K. J. Loh, F. Azhari, *Journal of Materials* **2012**, 64, 793.
[21] J. Lee, S. Kim, J. Lee, D. Yang, B. C. Park, S. Ryu, I. Park, *Nanoscale* **2014**, 6, 11932.
[22] T. Yamada, Y. Hayamizu, Y. Yamamoto, Y. Yomogida, A. Izadi-Najafabadi, D. N. Futaba, K. Hata, *Nature Nanotechnology* **2011**, 6, 296.
[23] M. Bai, Y. Zhai, F. Liu, Y. Wang, S. Luo, *Scientific Reports* **2019**, 9, 1.
[24] S. Chun, W. Son, D. W. Kim, J. Lee, H. Min, H. Jung, D. Kwon, A.-H. Kim, Y.-J. Kim, S. K. Lim, C. Pang, C. Choi, *ACS Applied Materials & Interfaces* **2019**, 11, 16951.
[25] M. Amjadi, A. Pichitpajongkit, S. Lee, S. Ryu, I. Park, *ACS Nano* **2014**, 8, 5154.
[26] J. Ramírez, D. Rodriquez, A. D. Urbina, A. M. Cardenas, D. J. Lipomi, *ACS Applied Nano Materials* **2019**, 2, 2222.
[27] L. Wang, K. J. Loh, W.-H. Chiang, K. Manna, *Nanotechnology* **2018**, 29, 1.
[28] Y. Liu, M. Pharr, G. A. Salvatore, *ACS Nano* **2017**, 11, 9614.
[29] T. Ha, J. Tran, S. Liu, H. Jang, H. Jeong, R. Mitbander, H. Huh, Y. Qiu, J. Duong, R. L. Wang, P. Wang, A. Tandon, J. Sirohi, N. Lu, *Advanced Science* **2019**, 6, 1.
[30] S. Choi, S. I. Han, D. Jung, H. J. Hwang, C. Lim, S. Bae, O. K. Park, C. M. Tschabrunn, M. Lee, S. Y. Bae, J. W. Yu, J. H. Ryu, S.-W. Lee, K. Park, P. M. Kang, W. B. Lee, R. Nezafat, T. Hyeon, D.-H. K. Kim, *Nature Nanotechnology* **2018**, 13, 1048.
[31] K. S. Novoselov, V. I. Fal′ko, L. Colombo, P. R. Gellert, M. G. Schwab, K. Kim, *Nature* **2012**, 490, 192.
[32] Z. Yang, Y. Pang, X.-l. Han, Y. Yang, J. Ling, M. Jian, Y. Zhang, Y. Yang, T.-L. Ren, *ACS Nano* **2018**, 12, 9134.
[33] S. Liu, X. Wu, D. Zhang, C. Guo, P. Wang, W. Hu, X. Li, X. Zhou, H. Xu, C. Luo, J. Zhang, J. Chu, *ACS Applied Materials & Interfaces* **2017**, 9, 24148−24154.
[34] C. S. Boland, U. Khan, G. Ryan, S. Barwich, R. Charifou, A. Harvey, C. Backes, Z. Li, M. S. Ferreira, M. E. Möbius, R. J. Young, J. N. Coleman, *Science* **2016**, 354 1257.
[35] T. Yang, X. Jiang, Y. Zhong, X. Zhao, S. Lin, J. Li, X. Li , J. Xu, Z. Li, H. Zhu, *ACS Sensors* **2017**, 2, 967.
[36] Q. Liu, J. Chen, Y. Li, G. Shi, *ACS Nano* **2016**, 10, 7901.

[37] Y. Lee, J. Kim, H. Joo, M. S. Raj, R. Ghaffari, D. H. Kim, *Advanced Materials Technologies* **2017**, 2, 1.
[38] T. Ferguson, A. V. Rowlands, T. Olds, C. Maher, *International Journal of Behavioral Nutrition and Physical Activity* **2015**, 12, 42.
[39] S. Yao, P. Ren, R. Song, Y. Liu, Q. Huang, J. Dong, B. T. O'Connor, Y. Zhu, *Advanced Materials* **2020**, 32, 1.
[40] M. D. Thelen, J. A. Dauber, P. D. Stoneman, *Journal of Orthopaedic & Sports Physical Therapy* **2008**, 38, 389.
[41] K. Manna, L. Wang, K. J. Loh, W. H. Chiang, *Advanced Materials Interfaces* **2019**, 6,
[42] J. Oksa, O. Hämäläinen, S. Rissanen, J. Myllyniemi, P. Kuronen, *Aviation, Space, and Environmental Medicine* **1996**, 67, 1138.
[43] J. T. Han, J.-h. Lee, *The Journal of Physical Therapy Science* **2014**, 26, 921.
[44] I. K. Ahn, Y. L. Kim, Y.-H. Bae, S. M. Lee, *Evidence-Based Complementary and Alternative Medicine* **2015**, 2015, 7.
[45] A. M. Montalvo, E. L. Cara, G. D. Myer, *The Physician and Sportsmedicine* **2015**, 42 48.
[46] V. Donec, A. Kriščiūnas, *European Journal of Physical and Rehabilitation Medicine* **2014**, 50, 363.
[47] D. S. Holder, Electrical impedance tomography: methods, history and applications., Institute of Physics Publishing Bodmin, Cornwall, UK, **2004**.
[48] K. J. Loh, T.-C. Hou, J. P. Lynch, N. A. Kotov, *Journal of Nondestructive Evaluation* **2009**, 28, 9.
[49] B. Loyola, V. La Saponara, K. J. Loh, T. M. Briggs, G. O'Bryan, *IEEE Sensors Journal* **2013**, 13, 2357.
[50] T. N. Tallman, S. Gungor, K. W. Wang, C. E. Bakis, *Smart Materials and Structures* **2014**, 23,
[51] R. H. Smallwood, Y. F. Mangnall, A. D. Leathard, *Physiological Measurement* **1994**, 15, A175.
[52] T. d. C. Martins, A. K. Sato, F. S. Moura, E. D. L. B. Camargo, O. L. Silva, T. B. R. Santos, Z. Zhao, K. Möeller, M. B. P. Amato, J. L. Mueller, R. G. Lima, M. d. S. G. Tsuzuki, *Annual Reviews in Control* **2019**, 48, 442.
[53] B. H. Brown, *Journal of Medical Engineering & Technology* **2003**, 27, 97.
[54] C. J. Kotre, *The British Journal of Radiology* **1997**, 70, 200.
[55] A. Adler, R. Guardo, *IEEE Transactions on Medical Imaging* **1996**, 15, 170.
[56] A. Adler, W. R. B. Lionheart, *Physiological measurement* **2006**, 27, 25.

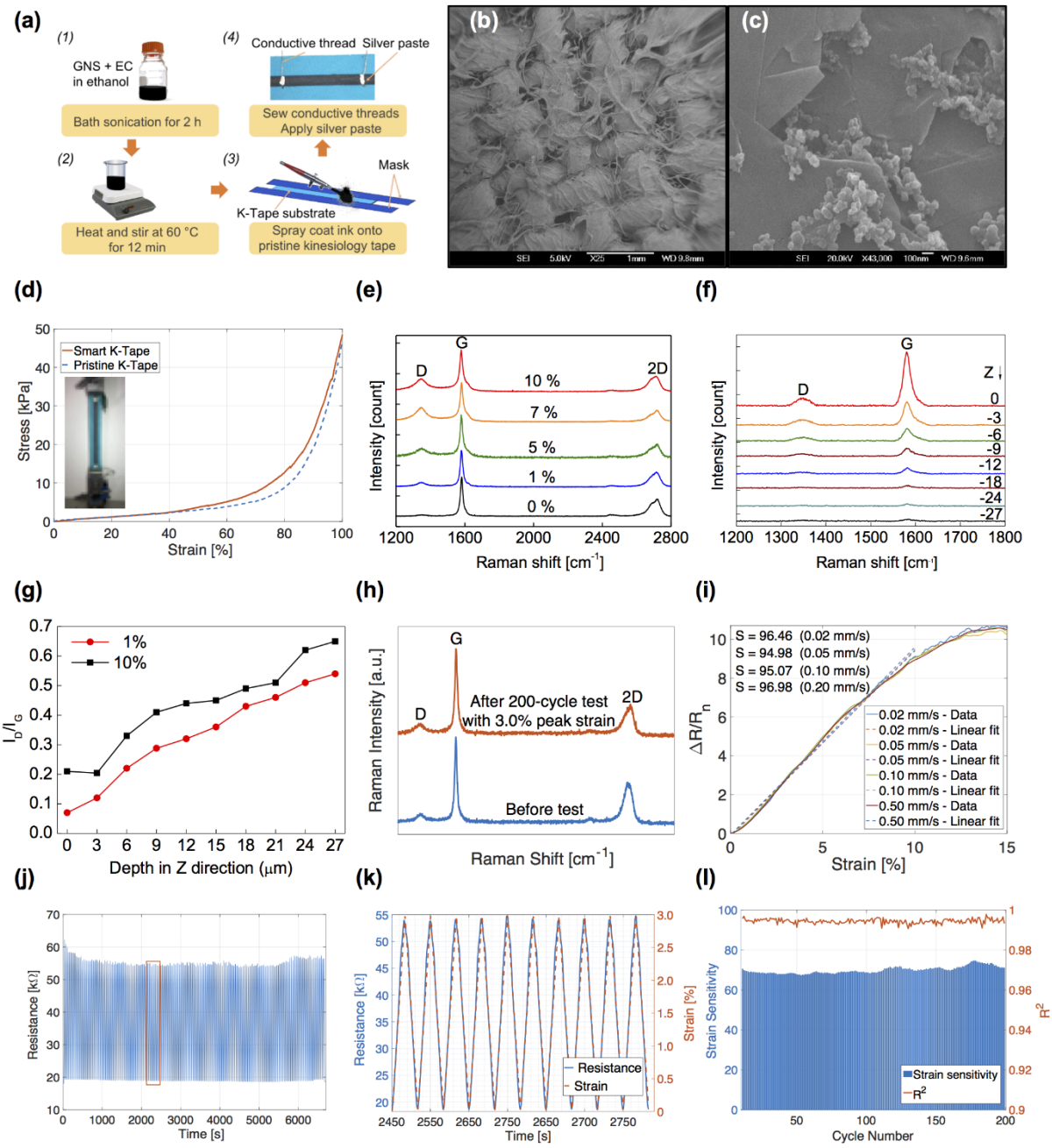

Figure 1. Material properties of Graphene K-Tape are examined by SEM and Raman spectroscopy, and the sensing performance of Graphene K-Tape are characterized. (a) The fabrication process of Graphene K-Tape is illustrated. An SEM image of the Graphene K-Tape surface shows (b) the nanocomposite coating individual fabric fibers and (c) at higher resolution the GNS morphology. (d) A comparison of stress-strain responses between bare K-Tape and Graphene K-Tape confirms that the film does not adversely affect mechanical properties of the fabric. The inset shows a Graphene K-Tape mounted in a load frame and stretched to 100%. (e) An overlay of Raman spectra corresponding to different magnitudes of applied uniaxial tensile strains shows that I_D/I_G decreases in tandem with increasingly applied tensile strains. (f) The Raman spectra of a Graphene K-Tape strained to 1% are probed at different Z depths, with Z=0 being the top surface of the film. (g) The I_D/I_G values are plotted as a function of depth when the specimen is strained to 1% and 10%. (h) Micro-Raman spectra of a Graphene K-Tape before and after 200 cycles of loading are shown. (i) An overlay of normalized change in resistance as a function of applied strain is plotted for four consecutive monotonic tensile tests conducted at

0.02, 0.05, 0.10, and 0.50 mm/s. A linear least-squares regression line is fitted to each curve up to 10% strain to estimate strain sensitivity. (j) A specimen is subjected to tensile cyclic load tests to a peak strain of 3%, and the electrical resistance time history is plotted. (k) A close-up view of a portion of its electromechanical response is shown and is overlaid with the applied strain pattern. (l) Linear fitting is performed for each of the 200 load cycles, and the strain sensitivities and corresponding R^2 values are plotted.

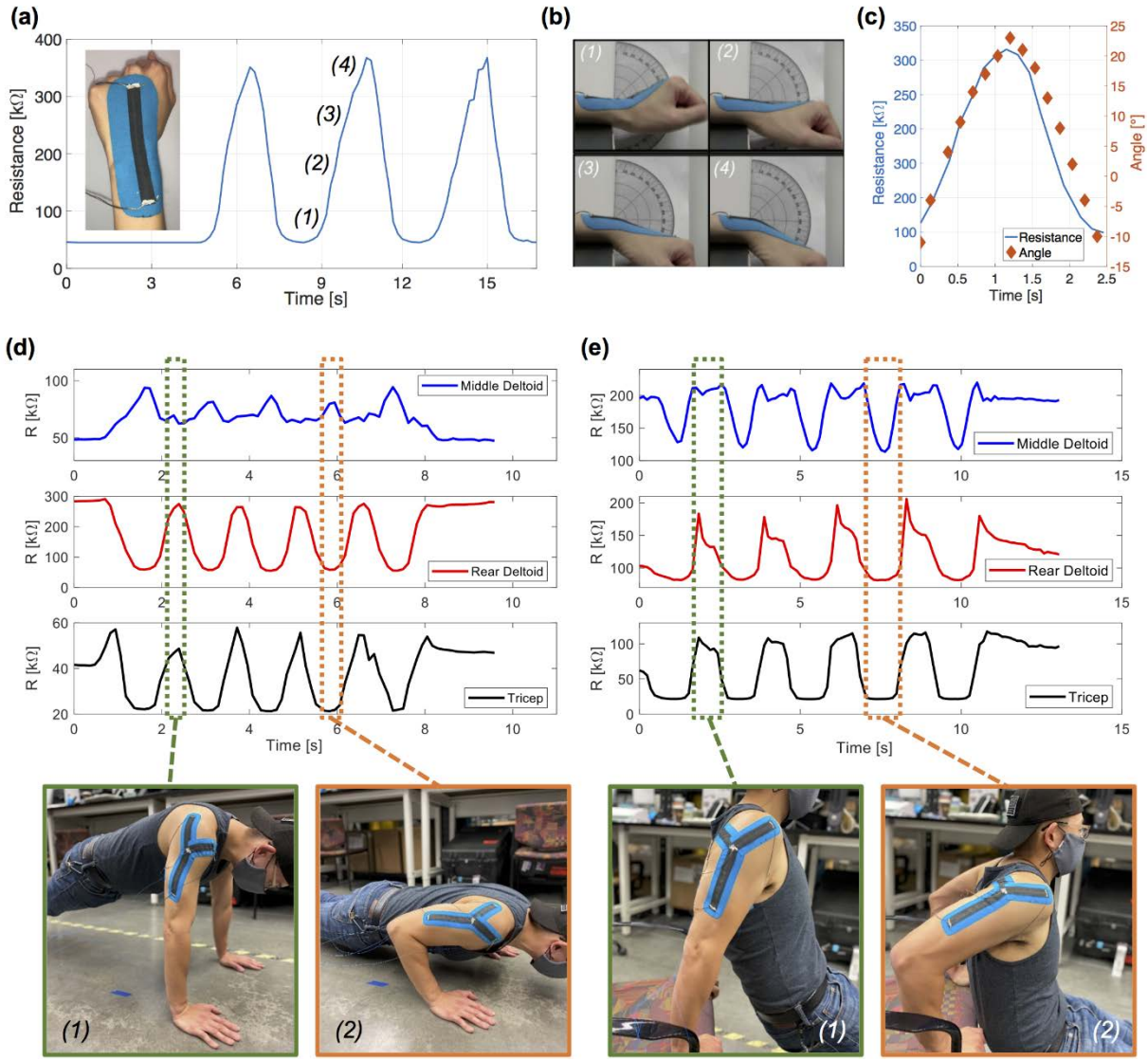

Figure 2. Human subject tests are conducted with the individual wearing Graphene K-Tapes on different parts of the body. (a) A Graphene K-Tape is affixed onto the subject's wrist, and the resistance time history recorded while the subject is performing repeated wrist bends is plotted. (b) Individual frames are extracted from video taken of the wrist bending test. (c) Image processing is employed to determine instantaneous wrist angles, and the results are overlaid with the Graphene K-Tape's resistance response, which shows good agreement. Human subject tests are also conducted with the individual wearing a network of three Graphene K-Tape sensors connected to form a 'Y' pattern on the upper-arm-shoulder region. The resistance time histories of the Graphene K-Tape network when the subject performed repeated (d) push-ups and (e) triceps dips are shown. Each sensing element in the network exhibits a unique waveform depending on whether the sensor is located over the middle deltoid, rear deltoid, or triceps.

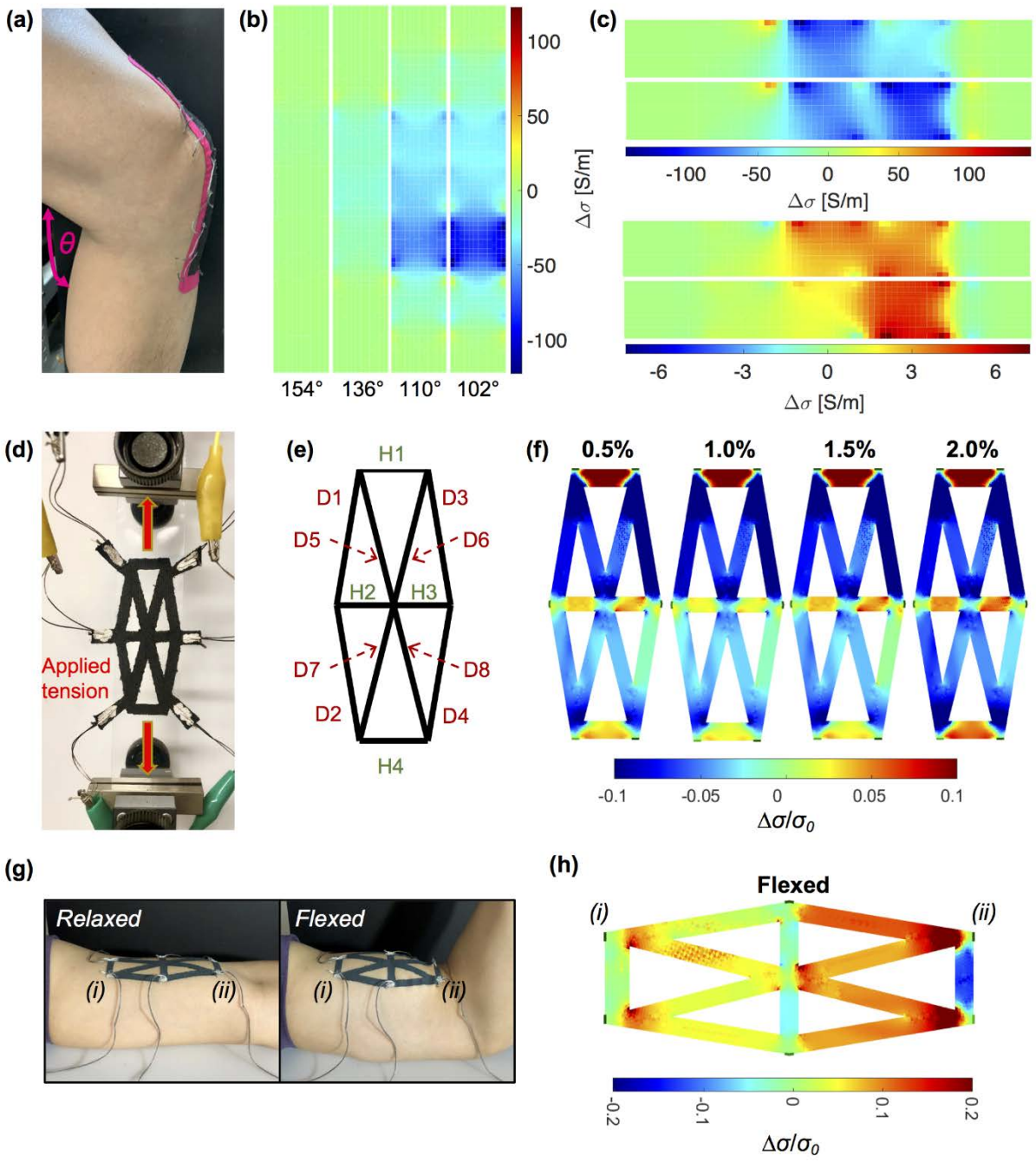

Figure 3. Continuous Graphene K-Tape and Graphene K-Tape Meshes are fabricated and tested to validate densely distributed strain sensing. (a) A Graphene K-Tape is adhered onto the knee of the subject. (b) A representative set of EIT results is shown. Each EIT image is the change in conductivity distribution of the specimen with respect to when the knee was unbent (θ=180°). Localized decreases in conductivity due to greater tension induced during knee bending are observed. (c) EIT successfully captures the magnitudes and locations where localized compressive and tensile strains are induced during wrist bending motions. (d) A Graphene K-Tape Mesh is affixed onto a PET substrate and mounted in a load frame for monotonic, uniaxial, tensile testing. (e) Each of the 12 struts is labeled accordingly, where 'H' stands for horizontal and 'D' stands for diagonal. (f) EIT is used to reconstruct the change in conductivity distribution (with respect to its unstrained state) of the specimen when subjected to different strain states (0.5% to 2.0%). (g) Human subject tests are performed by affixing a Graphene K-Tape Mesh onto the biceps area. EIT is used to interrogate the specimen while the subject performed a

controlled curling motion. (h) The normalized change in conductivity distribution when the subject's biceps are flexed (with respect to the relaxed state) is shown.